

Bottom simulating reflectors in the Manila Trench forearc and its implications on the occurrence of gas hydrates in the region

E.J.M. Maglalang^a, L.T. Armada^{a,*}, M.C. Santos^a, K.F. Sayen^a, C.B. Dimalanta^a, S.-K. Hsu^b, G.P. Yumul Jr.^c

^a Rushurgent Working Group, National Institute of Geological Sciences, University of the Philippines, Diliman, Quezon City, Philippines

^b Department of Earth Sciences, National Central University, Zhongli District, Taoyuan City, Taiwan

^c School of Environmental Science and Management, University of the Philippines, Los Baños, Philippines

ARTICLE INFO

Keywords:

Bottom simulating reflector
Manila trench forearc
Luzon
Gas hydrates

ABSTRACT

Gas hydrate occurrence and stability in active plate margins have been reported in various localities, with investigations focusing on its potential as an alternative energy resource or the threat it poses due to dissociation and methane release into the atmosphere. The Manila Trench forearc, proximal to active margins and probable methane-rich sediments, can be an analog for gas hydrate formation and geologic preconditions constrained by tectonics and sedimentation processes. The possible occurrence of gas hydrates in offshore western Luzon Island is reported for the first time based on bottom simulating reflectors (BSRs) in multi-channel seismic reflection datasets. Results indicate a prevalence of BSRs on the frontal wedge seaward of the North Luzon Trough (NLT) and in the West Luzon Trough (WLT) basin fill. Continuous, discontinuous, double, and plumbing BSRs in the forearc encompass a total area of approximately 15,400 km² at depths of 223–553 mbsf in the frontal wedge and 486 to 1428 mbsf within the basins. Enhanced amplitude reflectors (EARs) above and below the BSRs indicate possible gas hydrate and free gas accumulations, respectively. Gas chimneys associated with the upward migration of methane-rich fluids appear to be controlled by deep structural features. The accretion of continent-derived sediments along the northern segment of the frontal wedge promotes the formation of fluid migration structures, enhancing fluid migration and gas hydrate formation at shallower depths. Estimated geothermal gradient values for the frontal wedge range from 28 to 92 °C/km, consistent with previously reported in-situ measurements from offshore SW Taiwan. In contrast, arc-derived sediments within the NLT and west-ward fluid migration along the landward-tilted sequences limit gas hydrate accumulation within the basin. To the south, the preferential formation of gas hydrates within the WLT basin points to deep gas sources within the forearc basin sediments, with upward movement of methane-rich fluids along normal faults. Estimated geothermal gradient values in the basin are lower, ranging from 12 to 45 °C/km, reflecting lower thermal conditions. The absence of BSRs seaward of the WLT signifies widespread gas hydrate dissociation in the frontal wedge slope.

1. Introduction

The growing global demand for energy has prompted an intensified search for hydrocarbon resources, from traditional fossil fuels to unconventional ones such as gas hydrates. Interest in gas hydrates lies in the significant carbon volume that may be extracted from these deposits. Hydrate-related gas resources are estimated to be between 10¹³ m³ and 20 × 10¹⁵ m³ globally (e.g., Kvenvolden, 1993; Sain and Gupta, 2012; Portnov et al., 2019; Nasif et al., 2020). Despite being an attractive

alternative energy source, previous works have also emphasized its potential to trigger significant geologic hazards associated with gas hydrate dissociation and leakage into the environment. The release of methane trapped in the clathrate structure of gas hydrates has implications for the global greenhouse gas budget, and its impact on global warming is reportedly 25 times worse than that due to carbon dioxide (Demirbas, 2010). Gas hydrate dissociation may also fluidize sediments at the base of the gas hydrate stability zone (BGHSZ), triggering submarine slope failures and consequent tsunamis (Sain and Gupta, 2012).

* Corresponding author.

E-mail address: ltarmada@up.edu.ph (L.T. Armada).

<https://doi.org/10.1016/j.marpetgeo.2023.106538>

Received 14 March 2023; Received in revised form 30 September 2023; Accepted 4 October 2023

Available online 11 October 2023

0264-8172/© 2023 Elsevier Ltd. All rights reserved.

Nixon and Grozic (2007) reported that increased pore pressure due to gas hydrate dissociation may contribute to slope failure. However, whether this process alone can cause large-scale slope failure is unclear. More recent studies in the South China Sea infer that gas hydrate dissociation significantly contributes to slope destabilization. In the Shenhu area, the work of Wan et al. (2022) showed that overpressure associated with fluid migration along a gas column triggered submarine slope failure. The gradual dissociation of gas hydrates after this mass wasting event is inferred to have increased the pore pressure and decreased the shear strength within sediments, inducing a subsidiary slope failure (Wan et al., 2022). Another study in the Northern South China Sea was able to correlate periods characterized by pervasive gas hydrate dissociation and submarine landslide events using foraminifera and geochemical records from cores (Huang et al., 2022).

Gas hydrates are naturally occurring, ice-like substances that form when hydrocarbon gases (typically methane) become trapped within molecular hydrate cages, creating clathrate structures formed under low temperature and moderate to high-pressure conditions near the seafloor. These deposits are usually found in sedimentary sequences along continental margins and permafrost regions (Kvenvolden, 1988). The geothermal gradient and pressure regime under which hydrate stability for gas is met is known as the gas hydrate stability zone (GHSZ) (Sloan, 1998). Gas hydrate stability is further influenced by hydrocarbon gas composition, the presence of hydrate-forming components such as CO₂ and H₂S, and fluid salinity (Bohrmann and Torres, 2016). Hydrocarbon sources are often considered thermogenic or biogenic (Kvenvolden et al., 1984). Thermogenic gas hydrates form through the thermocatalytic breakdown of organic matter in sedimentary units found at depths greater than 1 km below the seafloor (Floodgate and Judd, 1992; Dhakal and Gupta, 2020). On the other hand, biogenic gases are generated through the microbial decomposition of organic matter at shallow intervals (<1 km) (e.g., Tissot and Welte, 1984; Meslé et al., 2013; Zhang et al., 2020). However, secondary microbial hydrocarbon generation at greater depths has also been documented, attributed to the biodegradation of a deeper oil pool or the reintroduction of a microbial community to organic-rich intervals (Katz, 2011). An example in the South Caspian basin shows dominant biogenic gas concentrations that do not correlate with depth, indicating ex-situ generation and migration (Katz et al., 2002).

The presence of gas hydrates is commonly indicated by bottom-simulating reflectors (BSRs) on seismic sections. The BSRs, which often coincide with BGHSZ are characterized by a reversed reflection polarity with respect to the seafloor (Chi et al., 1998; Geissler et al., 2014). The negative impedance contrast is formed by the transition from the higher seismic velocities of gas hydrate-bearing sediments to lower compressional seismic velocities of the underlying free gas-bearing sediments (Shipley et al., 1979). However, there are cases where BSRs only indicate the presence of free gas below the gas-hydrate stability zone and thus only imply the potential occurrence of gas hydrates above the BSR (Riedel et al., 2010). As such, BSRs are often not conclusive indicators of the concentration and volume of gas hydrates (e.g., Yuan et al., 1999; Chen et al., 2007). The BSRs usually mimic the seafloor bathymetry at constant depths and, in most cases, cross-cut strata (Mishra et al., 2020). In the Gulf of Mexico, Shedd et al. (2012) were able to document three types of BSRs: (1) continuous BSRs, which are coherent and continuous reflectors that mimic seafloor bathymetry; (2) pluming BSRs, which are continuous BSRs warped upward due to strong vertical fluid flux; and (3) discontinuous BSRs, which are not manifested as actual reflections but described as virtual subseafloor horizons delineated by the alignment of terminations of separate high-amplitude reflections. Double BSRs have also been documented in different locations, such as in Norway (Posewang and Mienert, 1999), in the Dongsha region in the northern South China Sea (Li et al., 2015), in the Kutei basin offshore Indonesia (Zhang et al., 2018), in the Nankai Trough, Japan (Foucher et al., 2002) and the northern Manila Trench accretionary prism near Taiwan (Wu et al., 2005). Double BSRs refer to two

negative polarity reflectors occurring subparallel to the seafloor at different depths. These features are attributed to either changes in stability conditions or the formation of hydrates from mixed biogenic and thermogenic hydrocarbon sources (Foucher et al., 2002; Golmshok and Soloviev, 2006).

The occurrence of gas hydrates in passive margins has been widely studied, as seen from extensive literature (e.g., Kvenvolden, 1993; Berndt et al., 2019; Liang et al., 2019). However, hydrate occurrence in active margins is also of interest, as subduction zones, particularly in the forearc region, are significant sinks for sediments and organic material from terrestrial source regions. Matsumoto et al. (2011) suggested that forearc basins are favorable sites for accumulating petroleum and gas hydrates. These deposits have been reported in several forearc basins, such as the Kumano Basin of the Nankai Trough (Taladay et al., 2017), the Sanriku-oki Basin in Northeast Japan (Kret et al., 2020), offshore east North Island of New Zealand (Rogers et al., 1999), and the Cascadia Margin (Reed et al., 2002). Gas hydrate accumulation in such basins has been widely attributed to extensive fluid migration in 1) landward-dipping strata, a characteristic element in compressional accretionary prisms, and 2) faults or fractures formed by increased tectonic activity in the accretionary prism (Hyndman and Davis, 1992). Natural gas exploration has had a breakthrough over the past two decades based on the theory that natural gas migration and accumulation are controlled by thermal fluid uplifting and are often associated with mud diapirs (He et al., 2016).

In the South China Sea region, gas hydrate research has mostly been done on the southeast margin of the Eurasian continent and the fold-and-thrust belt of the incipient arc-continent collision in offshore Southwest Taiwan. Various gas hydrate indicators have been extensively reported there, including BSRs, enhanced amplitude reflectors (EARs), blanking zones, and associated fluid migration pathways (mud diapirs and mud volcanoes, pockmarks, gas chimneys, seafloor methane venting) (e.g., Wu et al., 2005; Chen et al., 2014; Li et al., 2015; Lu et al., 2017; Berndt et al., 2019; Dirgantara et al., 2020). In offshore Southwest Taiwan, recent results of gas hydrate exploration have led to the first successful collection of shallow gas hydrate samples along the compressional ridges within the incipient arc-continent collision zone in the northern termination of the Manila Trench (Huang et al., 2021).

Despite the extensive gas hydrate research done in the northern termination of the Manila Trench offshore SW Taiwan, the long history of energy resource exploration in the Philippines has focused mainly on the offshore northwest Palawan area and several sedimentary basins. To date, no systematic study has been conducted to determine if gas hydrates are present in the offshore margins of the Philippines. This is the first study that examines the Manila Trench region for indicators of gas hydrate accumulation. This current investigation serves as a groundwork for future gas hydrate research in the country, with interest in its potential as an energy resource and in the geologic hazards associated with gas hydrate dissociation in an active margin setting, such as submarine slope failures and methane release to the atmosphere. This study re-interprets existing multi-channel seismic reflection data from the Manila Trench area to delineate BSRs, important seismic markers of probable gas hydrate occurrence. The heterogeneous character of the subducting South China Sea in terms of seafloor relief and thickness of sedimentary cover influences the deformation patterns along the Manila Trench subduction zone. This research will also explore the effects of this along-trench heterogeneity in the occurrence of gas hydrate indicators.

2. Geologic setting

The Manila Trench is an east-dipping, active convergent plate margin between the South China Sea basin and the Philippine Mobile Belt (Fig. 1). It stretches from 20° to 13°N latitude. It continues northward into the incipient arc-continent collision in offshore Southwest Taiwan. Its southern termination is defined by the Palawan-Central Philippine

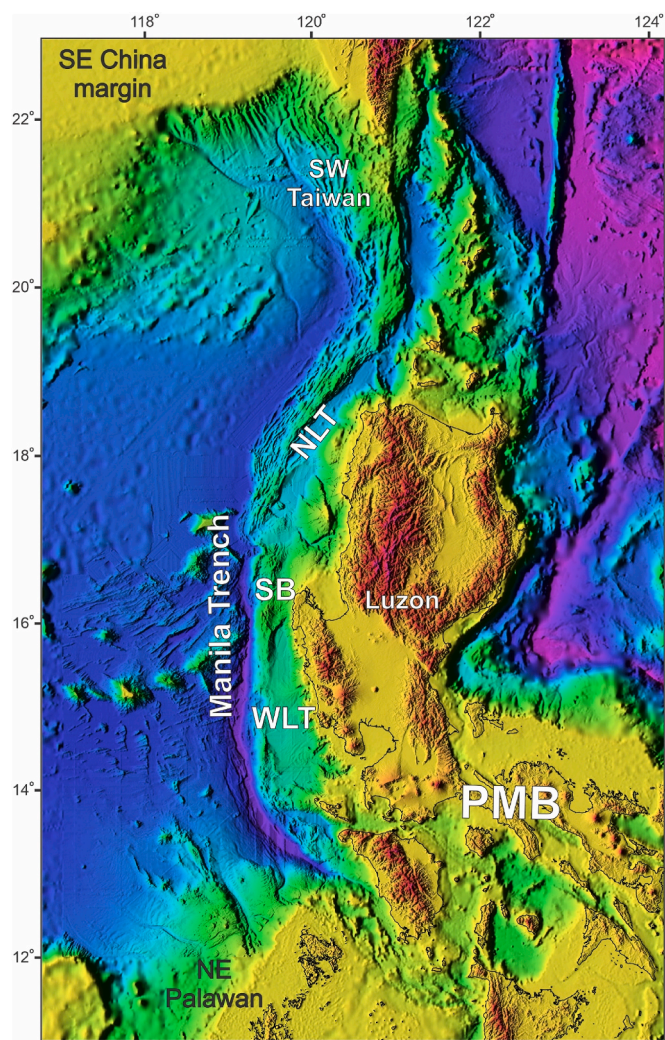


Fig. 1. Map of the Manila Trench region showing the offshore tectono-geomorphic features. NLT = North Luzon Trough. WLT = West Luzon Trough. SB = Stewart Bank. PMB = Philippine Mobile Belt.

Collision zone (Yumul et al., 2008). A bend in the trench axis can be observed at $\sim 20^\circ\text{N}$ latitude, attributed to a buoyant plateau's collision and partial subduction (Bautista et al., 2001) (Fig. 1). Due to this bathymetric high, a shallow dip of the subducting slab is observed in the northern segment of the Manila Trench. To the south, at $\sim 14^\circ\text{N}$ latitude, the trend of the trench axis changes from N-S to NW-SE and extends southeastward to the arc-continent collision zone in Central Philippines (e.g., Karig, 1983; Hayes and Lewis, 1985; Yumul et al., 2003). The dip of the subducting slab at the southern segment is steeper, reaching almost 90° at 13°N latitude (Yang et al., 1996). This variation in the slab dip is attributed to the slab tear along an extinct spreading center, the Scarborough Seamount Chain (Bautista et al., 2001; Fan et al., 2016). Intermediate-depth earthquakes observed in the southern Manila Trench exhibit down-dip extensional stress patterns that indicate that the observed dip steepening is caused by the negative buoyancy of the slab (Chen et al., 2015).

The age of initiation and rate of subduction along the Manila Trench varies. Karig (1983) suggested a Late Miocene initiation of subduction based on the radiometric dating of volcanic rocks and seismic correlation. However, Hayes and Lewis (1985) proposed a Late Oligocene to Early Miocene age coincident with the exhumation of the Zambales Ophiolite. Bellon and Yumul (2000) further support this by suggesting an Early Miocene onset using ^{40}K - ^{40}Ar dating of igneous rocks and

paleontological dating of sedimentary formations in the Baguio District. An Early to Middle Miocene age is consistent with the age of the volcanic belt along western Luzon (Yumul et al., 2003). A more recent geodynamic model by Huang et al. (2019) supports a Middle Miocene initiation of the Manila subduction zone. Karig (1983) suggested a rate of 5–6 cm/year, while Hayes and Lewis (1985) proposed a slow convergence rate of only 1 cm/year due to the collision between Taiwan and Eurasia. Hsu et al. (2012) utilized GPS data and estimated a convergence rate that decreases southward from 91 mm/yr north of Luzon to 55 mm/yr north of Mindoro.

The northern segment of the Manila Trench is characterized by a thick accretionary wedge formed from the accreted trench and seafloor sediments. The Manila Trench sediment infill consists of clastic turbidites with sediment thicknesses ranging from 250 to 2600 m (Lewis and Hayes, 1984). Gravity-controlled processes and longitudinal sediment transport supply these from two collision zones, the uplifted Eurasia/Taiwan collision zone in the north and the arc-continent collision zone in Central Philippines in the south (Lewis and Hayes, 1984). The southern segment of the trench is regarded as a mainly erosive margin caused by a sparser sediment supply (Armada et al., 2020).

The forearc basins that comprise the Manila Trench subduction zone are the North Luzon Trough (NLT) and the West Luzon Trough (WLT), separated by the Stewart Bank at $\sim 16^\circ\text{N}$ latitude (Fig. 1). Sediment infill of the basins are sourced from the Luzon volcanic arc. A major structural feature observed is the landward tilting of strata due to the uplift of the accretionary prism. The NLT is an asymmetric basin filled with 2.4–4 km thick sediments. The sediment fill consists primarily of turbidites, seen as laterally continuous reflectors in seismic sections (Lewis and Hayes, 1984). The WLT is characterized by a southward sloping seafloor, reaching ~ 3000 m deep west of Manila Bay, with a maximum sediment thickness of ~ 4.5 km (Lewis and Hayes, 1984). Basin sediments are likely sourced from the frontal wedge to the west and the Bataan Volcanic Complex immediately to the east of the basin (Armada et al., 2020).

3. Data and methods

3.1. Multi-channel seismic reflection data

Available multi-channel seismic (MCS) reflection datasets from the Manila Trench forearc region are utilized in this study (Fig. 2). Seismic profiles from the 1980 R/V VEMA (V3613) expedition in the Philippine Sea and South China Sea Basin were obtained from the Marine Geoscience Data System database portal as SEG-Y files (Hayes, 2015). The data obtained from the MGDS have been subjected to stacking and post-processing. A more recent marine survey was conducted within the Manila Trench region in 2014 using the R/V Ocean Researcher V (ORV-41) of the Taiwan Ocean Research Institute. The ORV-41 cruise collected approximately 1200 km of 24-channel seismic reflection data. Processed seismic profiles were obtained as SEG-Y and image files. Data treatment of the ORV-41 files was conducted in ProMAX following the processing flow of Armada et al. (2020) with a bandpass filter of 10–15–60–130 Hz and minimum phase predictive deconvolution. Normal move-out correction, stacking, and F–K migration were also carried out using a constant seawater velocity of 1480 m/s. The survey parameters of the ORV-41 and V3613 seismic surveys are shown in Table 1. Replotting and image enhancement of the seismic profiles were performed using the IHS Markit Kingdom software.

3.2. Bathymetry

The bathymetry data used in this study is sourced from the SRTM30_PLUS Global 1-km Digital Elevation Model (DEM), a global terrain model for ocean and land at 30 arc-second intervals (Sandwell et al., 2014). A more detailed bathymetry (~ 210 m resolution) from the National Mapping and Resource Information Authority (NAMRIA) is

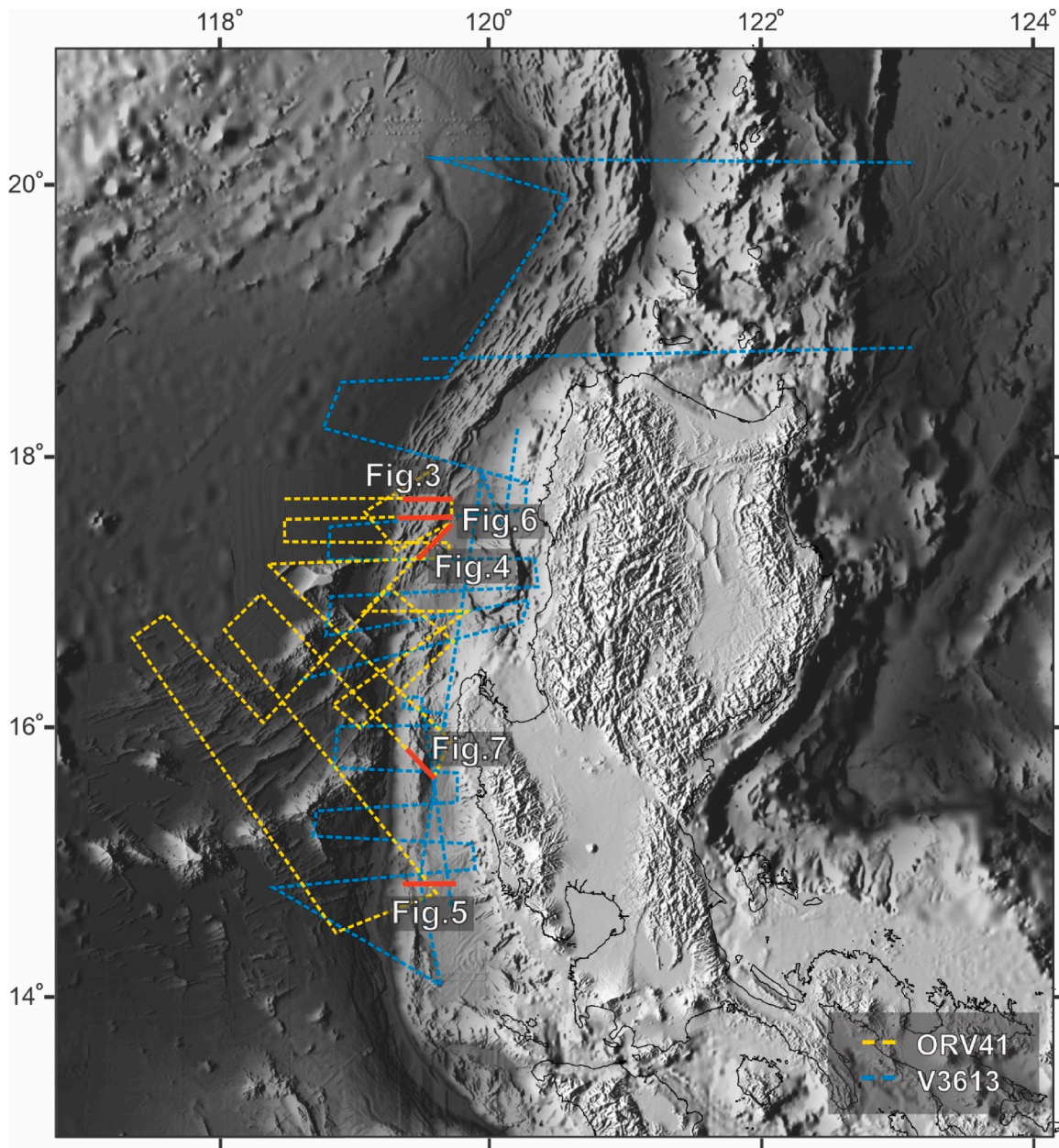


Fig. 2. Location of the multi-channel seismic survey lines along the Manila Trench forearc region. The seismic data sets are from the marine surveys of R/V VEMA (V3613) obtained from the Marine Geoscience Data System database portal (Hayes, 2015) and of R/V Ocean Researcher V (ORV-41).

also used to analyze seafloor features in offshore western Luzon.

3.3. BSR-derived geothermal gradient

BSR-derived geothermal gradient values were also calculated following the methodology of Li et al. (2015) using Equation (1).

$$G = \frac{T_{bsr} - T_{sf}}{D_{bsr}} \quad (1)$$

where G is the geothermal gradient ($^{\circ}\text{C}/\text{km}$), T_{bsr} is the temperature at the BSR depth ($^{\circ}\text{C}$), T_{sf} is the temperature at the seafloor ($^{\circ}\text{C}$), and D_{bsr} is the depth of the observed BSR (in kilometers below the seafloor, kmsf).

T_{sf} is estimated from the empirical relationship between bottom water temperature and seafloor depth using a power equation (Equation (2)) generated from the XBT measurements collected during the 2022 R/V Legend expedition in the Manila Trench region (Fig. 3).

$$T_{sf}(D) = 1693.7 \times D^{-0.857} \quad (2)$$

where T_{sf} is the bottom water temperature ($^{\circ}\text{C}$), and D is the seafloor depth in meters below sea level (mbsl).

T_{bsr} was calculated using the P-T equilibrium conditions for pure methane gas hydrates, using the logarithmic function of Wang et al. (2006) generated using the CSMHYD program (Equation (3)).

$$T_{bsr}(D) = 9.1256 \times \ln(D) - 50.029 \quad (3)$$

where T_{bsr} is the temperature of gas hydrate stability ($^{\circ}\text{C}$) for a pure methane gas hydrates at depth D (mbsl).

4. Results

The 2D seismic reflection profiles from the R/V VEMA and R/V Ocean Researcher V expeditions were examined to identify,

Table 1

Data acquisition parameters during the seismic surveys carried out by the R/V VEMA and R/V Ocean Research 5.

Acquisition vessel	R/V VEMA	R/V Ocean Researcher 5
Cruise	V3613	ORV-041
Year	1980	2014
Category	Multi-channel seismic	Multi-channel seismic
Source	Air Gun (BOLT:1500C)	Air gun array
Source volume (in ³)	932	1275
Air pressure (psi)	2000	–
Shot interval	18–30 s (~ every 50 m)	15 s (~ every 35 m)
Source depth (m)	7–10	5
Receiver	Hydrophone streamer	Hydrophone streamer
No. of channels	12	24
Channel interval (m)	50	6.25
Cable length (m)	1200	1200
Streamer depth (m)	10	5
Sample rate (ms)	4	1
Recording length (s)	12	10

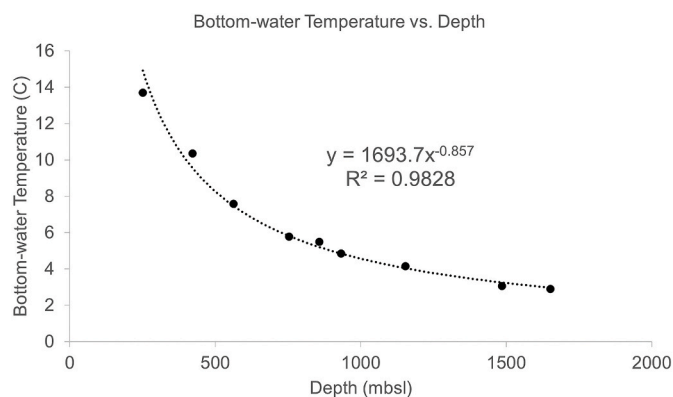


Fig. 3. Bottom-water temperature vs. depth curve generated from LGD2201 XBT data.

characterize, and delineate bottom-simulating reflectors and other seismic features in the Manila Trench region. The following criteria are used to identify Bottom Simulating Reflectors (BSRs) in the seismic sections: (1) strong and coherent reflectors showing reversed polarity concerning the seafloor (for continuous BSRs) or aligned terminations of separate, high amplitude reflections (for discontinuous BSRs); (2) reflectors which mimic the seafloor; (3) generally shallow events with gradually increasing sub-seafloor depth as water depth increases; and (4) reflectors which cross-cut stratigraphic bedding (Shedd et al., 2012). The presence of blanking zones characterized by reduced amplitudes and enhanced amplitude reflectors (EAR) with high amplitudes above and below BSRs has also been reported (Zhang et al., 2020). Double BSRs, two reflectors with reverse polarity occurring subparallel to the seafloor but at different depths, are also delineated in some seismic reflection profiles.

4.1. Continuous BSRs

Continuous BSRs, characterized by strong, coherent reflectors that mimic the seafloor bathymetry and frequently cut across strata, are the most widely observed BSR type in the Manila Trench forearc region. This BSR type occurs extensively in the northern frontal wedge and the WLT, with limited occurrence in the NLT.

A continuous BSR is observed in the Manila Trench accretionary prism, between CDP 6000 and 9000 (Fig. 4b). The BSR is observed between depths of 4s–4.25s (TWT) and extends laterally for about 20 km. The continuous BSR occurs at a relatively constant depth below the seafloor and cuts through preserved stratigraphic reflectors of the accreted trench infill. Above the BSR, observed EARs are interpreted to

be gas hydrate-rich horizons. The EARs found below the BSR are inferred to be free gas horizons. Several thrust faults cut through the BSRs and serve as conduits for upward fluid expulsion. A gas chimney is also observed along the profile, cutting through the sediments vertically (Fig. 4).

West of the thick frontal wedge, the North Luzon Trough (NLT) hosts limited occurrences of continuous BSRs. The BSRs are mostly found on the western boundary of the basin, transitioning into the accretionary prism. The NLT infill is characterized by parallel to sub-parallel, high amplitude reflectors, interpreted to be turbiditic sequences, that onlap onto the accretionary prism. A continuous BSR is observed in southern NLT, in an area traversed by a giant submarine canyon roughly trending E-W (Fig. 5). The BSR occurs between CDP 8500 to 10,500, extending laterally for about 10 km at a depth of 4s, hosted within an interval characterized by chaotic, low amplitude reflectors identified to be a mass transport deposit (Fig. 5). The BSR continues as a discontinuous BSR, defined by terminations of EARs. Unlike the BSR observed in the accretionary prism, this discontinuous BSR does not mimic the seafloor reflector and instead follows the boundary between the mass transport deposit and the overlying turbiditic sequences characterized by parallel to semi-parallel, high amplitude reflections. EARs are observed above and below the BSR, similar to the previous example. A reflector cut by the BSR shows a polarity reversal, indicating a transition from a gas hydrate-filled horizon to a free gas-filled horizon.

Widespread continuous BSRs were also observed within the West Luzon Trough (WLT) (Fig. 6). The BSR, observed between CDP 29500 and 30,500, at a depth of 4.3s, mimics the seafloor reflector at a relatively constant depth, sub-parallel to strata. Basin infill of the WLT is characterized by parallel to sub-parallel, moderate to high amplitude reflections occurring in a sub-horizontal manner and are most likely turbiditic. The BSR crosscuts onlapping sequences at the western portion of the basin.

4.2. Pluming BSRs

Within the northern segment of the accretionary prism, the widespread continuous BSRs extending laterally up to 15 km are sometimes deflected or warped upward due to strong vertical fluid flux, forming pluming BSRs (Fig. 7). This pluming BSR is observed between CDP 5250 and 5500 at a depth of 3.5s (TWT). Domal EARs underlie the BSR. These are interpreted to be gas-enriched sediments, influenced by fluid migration along the numerous thrust faults cutting through the frontal wedge.

4.3. Double BSRs

Double BSRs proximal to the Stewart Bank are observed in the northernmost portion of the West Luzon Trough. The double BSRs are observed within the basin infill overlying the flanks of the accretionary prism between CDP 1000 and 2800 (Fig. 8). These are separated by a vertical distance of 0.5s TWT and extend to approximately 20 km. The deeper BSR, or BSR 2, occurs between 3.4s and 3.8s. This deeper reflector is much less disrupted and defined by a coherent, reversed amplitude reflector with EARs occurring above and below the BSR. On the other hand, the shallower BSR 1 occurs between 2.9s and 3.2s. BSR 1 is more segmented compared to BSR 2, defined by the alignment of terminations of EARs. This implies that BSR 1 is likely discontinuous. The EARs are more concentrated proximal to BSR 1, occurring both above and below the reflector, which can be interpreted as gas hydrate and free gas horizons, respectively.

5. Discussion

5.1. Implications on gas hydrate occurrence

Analysis of multichannel seismic reflection data from the ORV-41

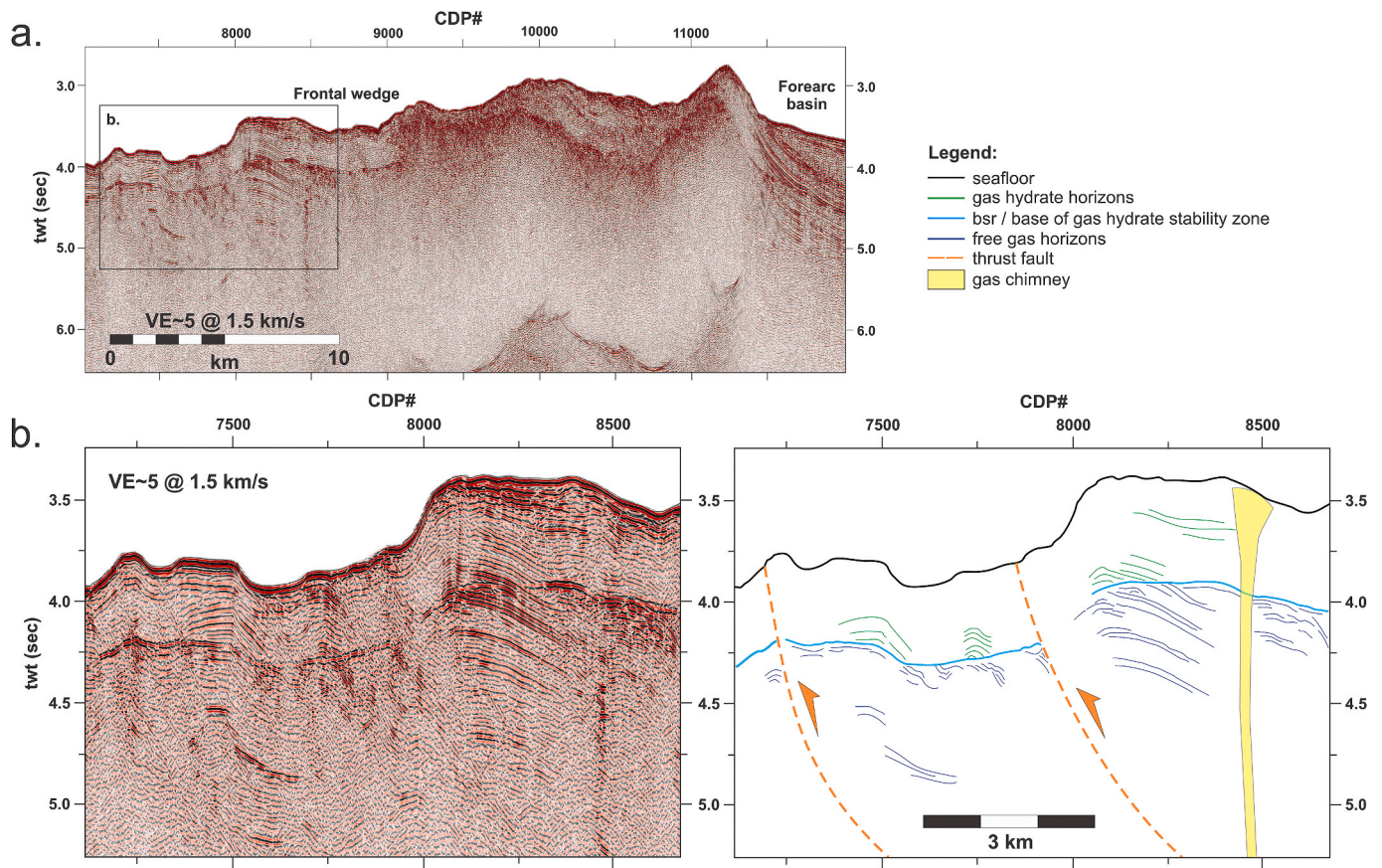


Fig. 4. (a) West-east seismic survey line from the frontal wedge to the forearc basin near the northern end of the Manila Trench. (b) Close-up view of the frontal wedge area. The interpreted seismic section shows a continuous BSR (light blue line), thrust faults, and a gas chimney. See Fig. 2 for the location of the survey line.

and V3613 surveys revealed the presence of BSRs in the Manila Trench forearc region. The BSRs were observed at depths varying from 223 to 553 mbsf in the frontal wedge and 486 to 1428 mbsf within the forearc basins, extending laterally from ~3 to 50 km. The inferred GHSZ encompasses a total area of about 15,400 km² in the study area (Fig. 9). Without drill data, it is challenging to constrain the lithology of the gas hydrate reservoirs and the saturation of the gas hydrate and free gas deposits. Seismic facies were determined based on the amplitude, continuity, polarity, and frequency of seismic reflectors and the geometry and terminations of the stratigraphic package to provide preliminary information on the possible lithologies hosting the gas hydrates. The seismic facies characterized by stratified, parallel to subparallel, continuous reflectors are identified to be turbiditic sequences. These seismic facies, observed in both the North Luzon Trough and West Luzon Trough, indicate that the sedimentary infill of the forearc basins is composed mostly of turbiditic sequences sourced from the Luzon arc. In the WLT, the continuous and double BSRs and EARs observed are hosted by these turbiditic sequences. In the NLT, BSRs can still be observed within turbiditic sequences. However, they are not as widespread as those observed in the WLT and tend to occur only at the western flanks of the basin, proximal to the accretionary prism. Aside from turbidite sequences, seismic facies characterized by low amplitude, chaotic, and contorted reflections are evident in the western portion of the NLT. These are believed to be mass transport deposits (MTDs) and may suggest episodes of submarine landslides sourced from the accretionary prism. The MTDs are also observed in the basin's southern part and may be attributed to the E-W submarine canyon system north of Lingayen Gulf. Continuous and discontinuous BSRs are also noted within some of these MTDs. They may indicate a possible coarser-grained reservoir for some gas hydrate deposits (Fig. 5). Hemipelagic sedimentation is suggested by the parallel to sub-parallel, continuous, low amplitude

reflections. These facies are generally undisturbed at the uppermost portions of the sedimentary basin sequence, often infilling erosion-related depressions at the upper parts of the accretionary prism. Gas hydrate-related features are not observed in these younger deposits.

Aside from seismic facies, bottom-simulating reflectors can also provide clues on the general type of sediments hosting the gas hydrates (Shedd et al., 2012). The BSRs observed in the Manila Trench forearc region are identified to be continuous BSRs. Continuous BSRs have been reported in generally homogenous lithologies that permit gas migration (Shedd et al., 2012). Due to the absence of drillhole data, a preliminary interpretation of the observed continuous BSRs in the Manila Trench area indicates that the gas hydrates may be hosted in homogenous lithologies that permit uniform gas diffusion, forming deposits with widespread distribution.

High amplitudes are good indicators of gas hydrate saturation. The EARs found above BSRs may indicate the presence of gas hydrates with >40% saturation (Boswell et al., 2016). Thus, moderate to high hydrate saturations may be present in the intervals characterized by higher amplitudes. Several seismic profiles showed strong or enhanced reflections immediately below the BSRs. These indicate the possible presence of gas-charged sediments. The EARs below BSRs in the Sanriku-Oki forearc basin along the Japan Trench have similarly been interpreted to correspond to methane gas (Eng and Tsuji, 2019). However, the saturation of the free gas accumulations is challenging to deduce using seismic data alone due to its amplitude insensitivity, with little free gas needed to produce high amplitudes (Boswell et al., 2016).

A combination of biogenic and thermogenic gas sources has been documented in active margins such as SW Taiwan (Dirgantara et al., 2020) and Eastern Nankai Trough (Suzuki et al., 2015). Organic matter undergoes a progressive transformation during burial, and at shallow subsurface depths, primary biogenic methane is produced by microbial

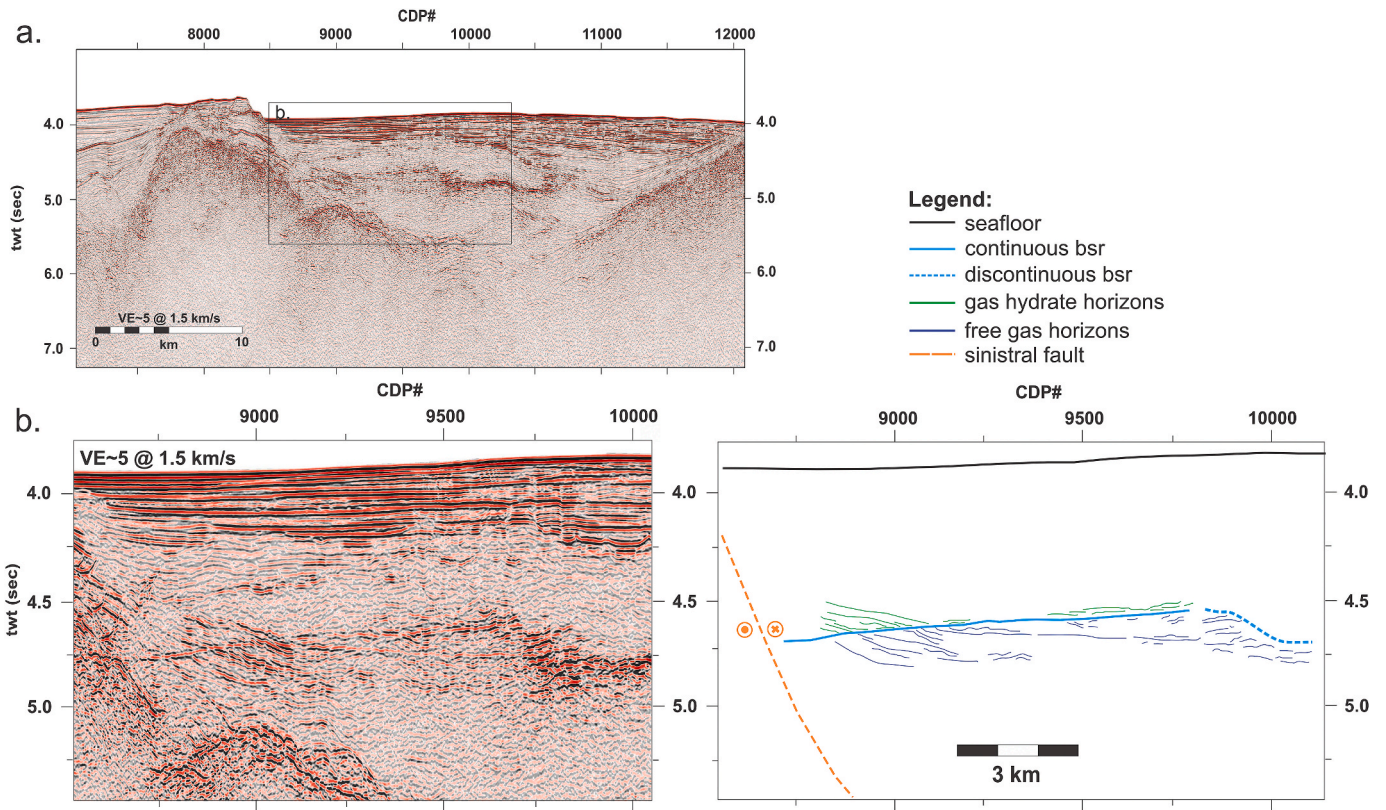


Fig. 5. (a) Northeast-southwest seismic survey line along the southern portion of the North Luzon Trough. (b). Close-up view of the basin infill. The interpreted seismic section shows a continuous and discontinuous BSR hosted within a mass transport deposit. See Fig. 2 for the location of the survey line.

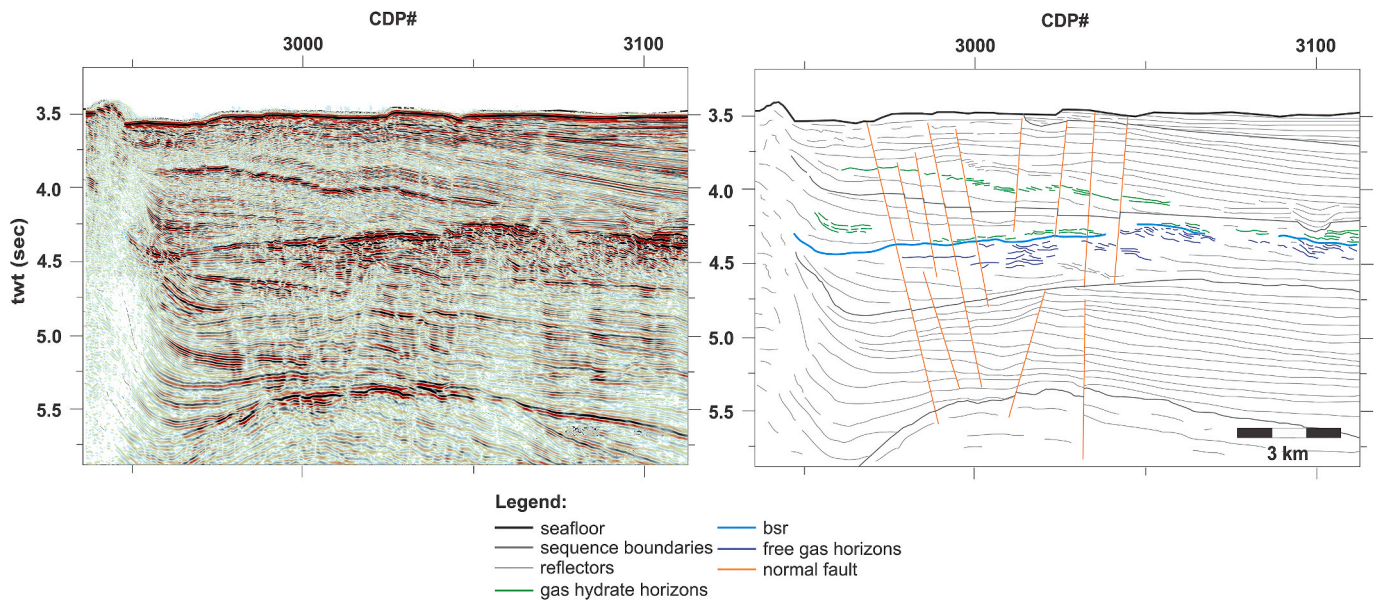


Fig. 6. Northwest-southeast seismic survey line along the northern portion of the West Luzon Trough. The interpreted seismic section shows a continuous BSR hosted by turbiditic sequences. Enhanced amplitude reflectors found above the BSR indicate the presence of gas hydrate intervals. See Fig. 2 for the location of the survey line. Modified from Arfai et al. (2011).

methanogenesis (Meslé et al., 2013). In the scheme of the thermal evolution of organic matter during burial, most microbial methane generation occurs at depths of less than 1 km, although deeper microbial generation has also been documented (Tissot and Welte, 1984; Katz et al., 2002; Katz, 2011; Meslé et al., 2013). The BSRs observed in the Manila Trench forearc region generally occur at shallow intervals (<1

km); thus, it is possible that in-situ biogenic methane may have been a source of gas during the formation of the gas hydrate deposits. Secondary microbial gases and, possibly, deeper thermogenic gas-rich fluids may have also been present during hydrate formation, both sourced from deeper sources that reach the gas hydrate stability zone through different fluid migration pathways, such as faults and gas chimneys.

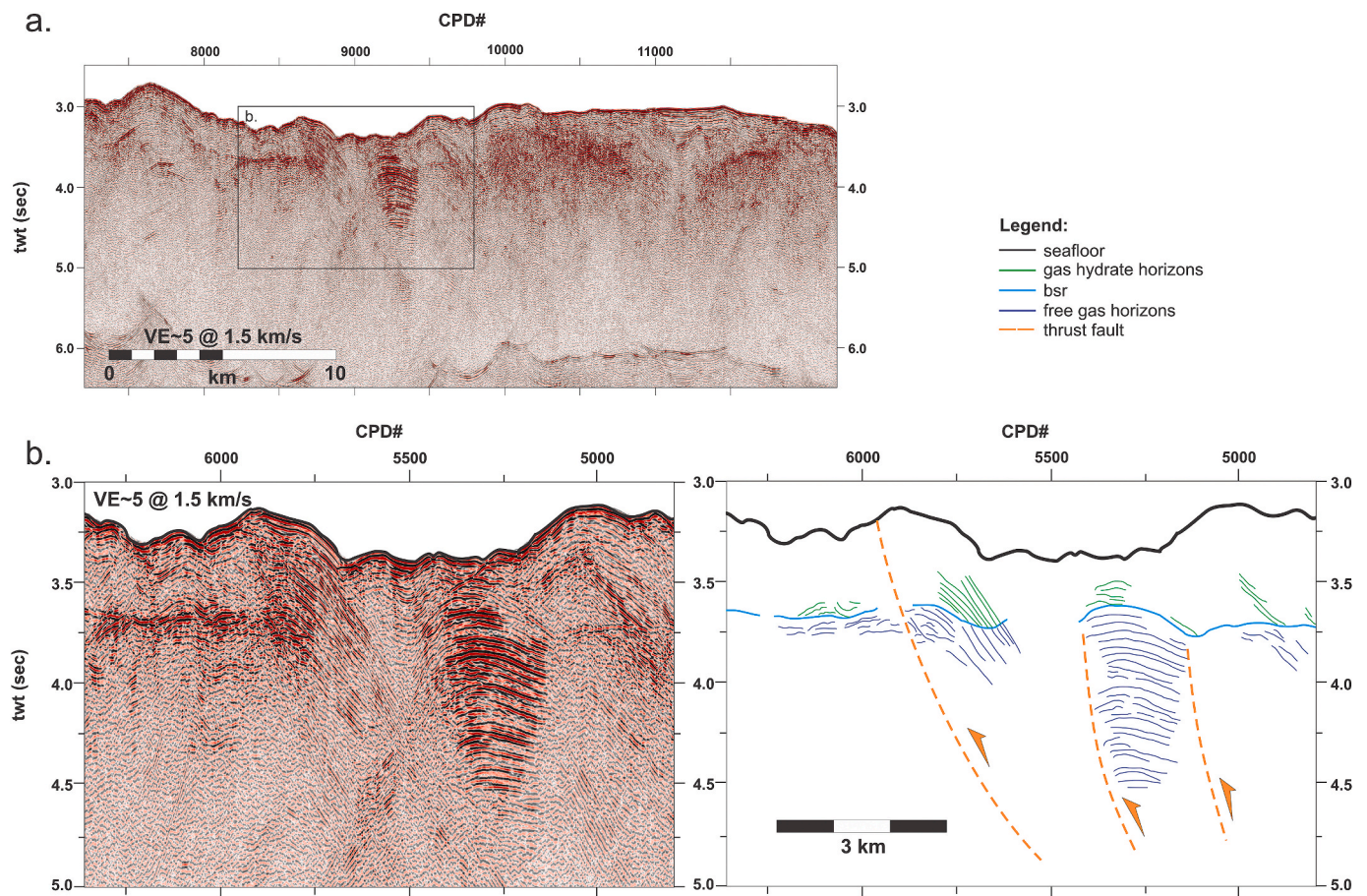


Fig. 7. (a) West-east seismic survey line along the frontal wedge. (b) Close-up view of the frontal wedge showing plumbing BSRs. Domal enhanced amplitude reflectors interpreted as gas-enriched sediments are found underlying the plumbing BSRs. See Fig. 2 for the location of the survey line.

Areas proximal to active fluid-escape structures have been attributed to higher concentrations of gas hydrates (Paganoni et al., 2018; Berndt et al., 2019). Compression drives fluid flow from the dewatering of sediments, which, as observed in other subduction zones, is attributed to porosity reduction with depth and distance from the toe of the wedge (Breen and Orange, 1992). Conversely, the potential fluid flow pathways in the forearc basin are the normal faults. These structural features would provide pathways for the gas hydrate migration, leading to free gas and gas hydrate accumulation (e.g., Miyakawa et al., 2014; Eng and Tsuji, 2019). Basement-involved normal faults can serve as conduits for focused fluid flow of biogenic and thermogenic methane to the gas hydrate stability zone, similar to the mechanism inferred for gas hydrate formation in the Dongsha region, South China Sea (e.g., Li et al., 2015). Additionally, the permeation of fluids along the land-dipping strata of the forearc basins might have also contributed to the thermogenic gas content of the gas hydrates.

Additional evidence of deeply-sourced gas influence in the study area includes the observed double BSRs and plumbing BSRs. Plumbing BSRs observed in the Manila trench accretionary prism indicate the influence of vertical fluid fluxes such as gas chimneys. In the northern portion of the WLT near Stewart Bank, seismic sections indicate the occurrence of double BSRs (Fig. 8). Double BSRs formed due to the influence of thermogenic gas sources typically indicate a layered gas hydrate structure configuration (Paganoni et al., 2018). The shallower BSR is associated with the base of the stability zone of pure methane hydrates of biogenic origin. In comparison, the deeper BSR is associated with the base of the stability zone of hydrates with larger gas molecules within the lattices, such as higher hydrocarbons sourced from thermogenic gas. Tinivella and Giustiniani (2013) showed that the difference between the depths of

double BSRs associated with biogenic and thermogenic hydrates is more than 200 m in shallow water depths. Thus, significant thermogenic gas contributions from deeper levels are possible considering the depth separation between the observed double BSRs of ~300–400 m. The fault separating the Stewart Bank and the WLT, combined with the numerous normal faults in the basin, may have served as primary fluid migration conduits. Thus, EARs observed above the shallower BSR 1 may correspond to biogenic pure methane hydrates (Fig. 8). In contrast, the EARs observed above BSR 2 possibly indicate the occurrence of thermogenic gas hydrates. It should be noted, however, that hydrate instabilities arising from disequilibrium conditions are also possible mechanisms of the double BSR formation, considering the active tectonics in the area. The double BSRs observed near Stewart Bank may indicate gas hydrate stability re-equilibration caused by rapid forearc uplift due to the reported subduction of an extinct spreading center.

The BSRs in the Manila Trench region indicate two possible accumulation sites of gas hydrates: within the accretionary prism and western flank of the NLT offshore Ilocos between 17°N and 18°N and in the sedimentary infill of the WLT (Fig. 9). The development of a high concentration of gas hydrates in the overlying sedimentary sequence requires upward fluid flow (Kvenvolden and McMenamin, 1980; Judd and Hovland, 2007). The possible migration pathways in the accretionary complex are the numerous thrust faults, mud diapirs, and gas chimneys. For the forearc basins, fluid migration is likely focused along normal faults and through permeation along tilted sedimentary infills.

BSR-derived geothermal gradient values were also calculated using the depths of observed BSRs along seismic profiles. Estimated geothermal gradient values for the accretionary prism in the northern forearc segment range from 28 to 92 °C/km, with an average of 55 °C/

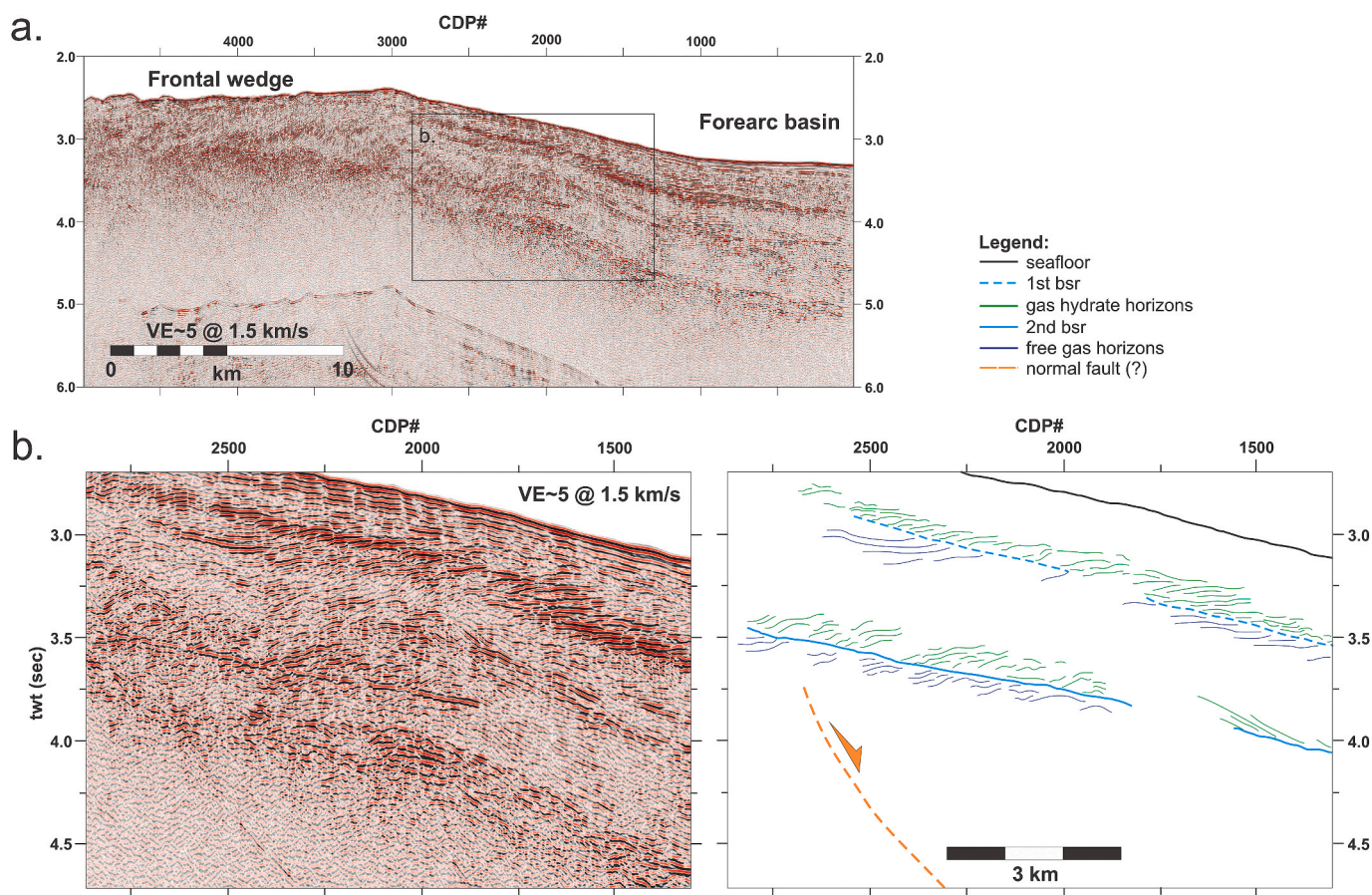


Fig. 8. (a) Northwest-southeast seismic survey line in the northern portion of the West Luzon Trough. (b) Close-up view showing the occurrence of double BSRs. See Fig. 2 for the location of the survey lines.

km. These measurements are consistent with in-situ geothermal gradient measurements obtained from the northern continuation of the trench in SW Taiwan, which range from 25 to 90 °C/km (Shyu et al., 2006; Liao et al., 2014), and with the BSR-derived geothermal gradient estimates of Li et al. (2015) for the same area, ranging from 20 to 100 °C/km, with an average of 48 °C/km. Within the WLT, the observed BSRs yield low geothermal gradient values, ranging from 12 to 45 °C/km, with an average of 26 °C/km. These estimates reflect the lower thermal conditions observed within the forearc basin, which is consistent with the previously reported low heat flow in the area, ranging from 5 to 60 mW/m², with an average of 30 mW/m² (Hayes and Lewis, 1985; Shi et al., 2003). These low thermal measurements might explain the deeper BSRs observed within the WLT. However, in the area south of the Stewart Bank, where double BSRs are observed, the shallower BSR 1 yielded high BSR-derived geothermal gradient values, unlike the typical measurements obtained from the WLT. Heat flow values derived from BSR 1 range from 23 to 60 °C/km, with an average of 51 °C/km, higher than the values obtained from WLT. In contrast, geothermal gradient values derived from the deeper BSR 2 range from 20 to 65 °C/km, with an average of 23 °C/km, closer to the estimates for the basin. The low measured heat flow values in the WLT indicate cooler conditions, which is consistent with the low geothermal gradient values estimated for the basin. These observations suggest that BSR 1 may not be in equilibrium with the current thermal conditions in the WLT and reflect current disequilibrium conditions, giving rise to double BSR formation.

5.2. Comparison of BSR characteristics in offshore Taiwan and western Luzon

Bottom simulating reflectors delineated in the seismic profiles

acquired along the Manila Trench forearc region were observed to have the same characteristics as the BSRs documented in the fold-and-thrust belts located offshore SW Taiwan. The presence of continuous and pluming BSRs was reported within these regions. The delineated BSRs can be noted at depths between 2.0s and 2.5s (TWT). Additionally, EARs found below continuous BSRs, gas chimneys related to pluming BSRs, and numerous faults were reported in offshore SW Taiwan.

Hsu et al. (2018) reported a prominent continuous BSR along the axis of Formosa Ridge about 2.0s–2.6s (TWT) below the seafloor that generally crosscuts flat-lying sedimentary strata. Below this continuous BSR, EARs are observed. Berndt et al. (2019) reported similar continuous BSRs at depths ranging from 2.0s to 2.5s (TWT) below the seafloor within the Formosa, Four-Way Closure, and Yuan-An ridges. The observed BSRs show strong reverse seismic polarity that crosscut sedimentary reflectors. Numerous thrust and normal faults and vent sites were also observed that serve as conduits of fluid migration.

Another type of BSR was also reported by Hsu et al. (2018) on the southern end of Formosa Ridge. A pluming BSR below the ridge floor was delineated at depths of 2.0s–2.5s (TWT) in the NT0705-F-22-23 seismic profile. Below this BSR is a vent structure that allows upward fluid migration represented by a vertical blanking zone. Han et al. (2019) also reported well-distributed pluming BSRs at the Pointer Ridge offshore SW Taiwan. The BSRs are observed below the seafloor at 2.0s–2.5s (TWT). The presence of gas chimneys as subsurface fluid pathways was also noted. These associated chimneys indicate the ongoing fluid flow at Pointer Ridge.

The reported BSRs in the Manila Trench forearc region and offshore Taiwan indicate the presence of gas hydrates, with gas sources often categorized as biogenic or thermogenic (Kvenvolden et al., 1984; Dhakal and Gupta, 2020). Dirgantara et al. (2020) inferred that a combination

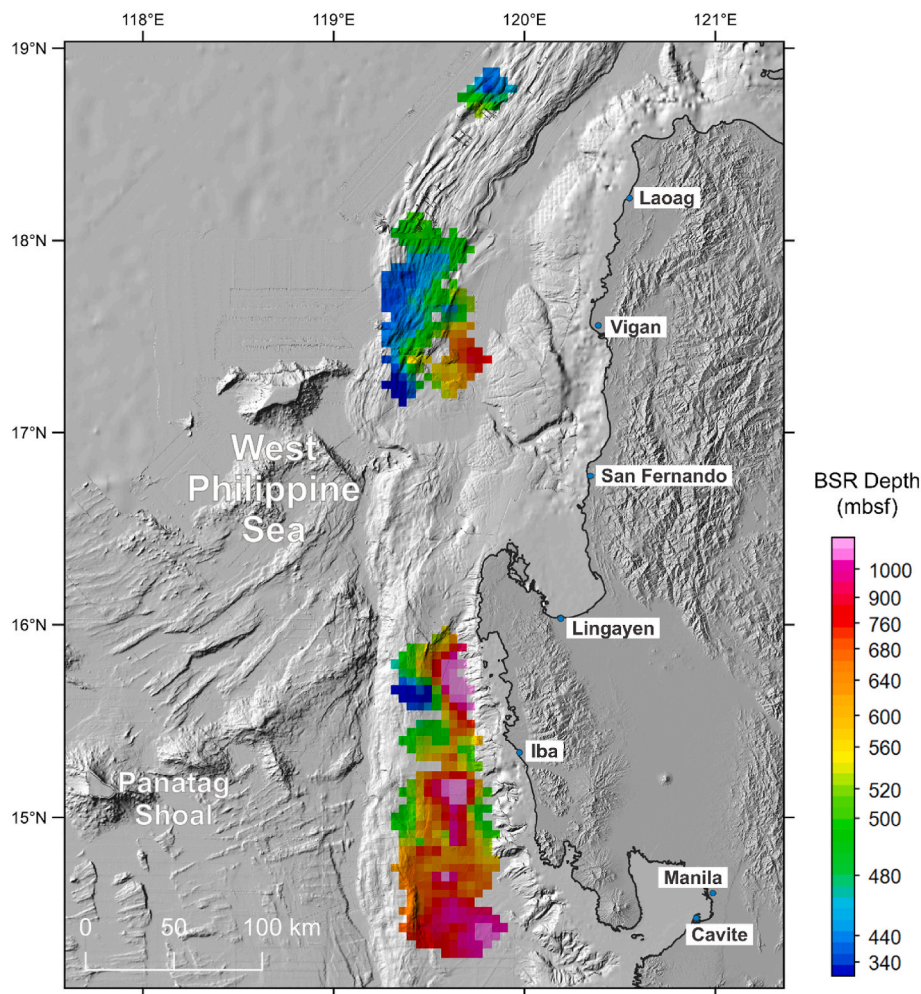


Fig. 9. Distribution of the BSR occurrences. Two possible accumulation sites of gas hydrates in the Manila Trench region include the accretionary prism and western flank of the North Luzon Trough offshore Ilocos between 17°N and 18°N and in the sedimentary infill of the West Luzon Trough.

of these gas sources occurs offshore southwest Taiwan. The delineated BSRs along the Manila Trench and offshore Taiwan regions are observed at relatively shallow depths, suggesting that biogenic methane may have been the source of gas hydrates. Thermogenic gas-rich fluids may have also been a possible gas source, evidenced by the reported pluming BSRs that indicate vertical fluid fluxes along gas chimneys. The normal and thrust faults observed within the forearc basins and ridges may also serve as additional migration pathways for the thermogenic gas sources.

5.3. Preconditions for gas hydrate formation in the Manila trench forearc region

Convergent margins like the Manila Trench subduction zone are conducive environments for gas hydrate formation due to the high sedimentation rates associated with intense tectonic activity. The compressional deformation along the active margin also generates pathways such as faults and gas escape structures along which gasses and fluids can migrate to the gas hydrate stability zone. Higher organic matter concentrations characterize these margins due to upwelling and recycled kerogen (Rajput and Thakur, 2016). Methane-rich fluid expulsion occurs during subduction, and faster sedimentation rates account for gas hydrates in active margins (Judd and Hovland, 2007; Ligtenberg, 2005). Accumulation of hydrates in active margins is enhanced in coarse clastic sediments with high permeability over accretionary regions (Hyndman et al., 1993).

Stevenson (1996) described the ideal characteristics for the most

favorable hydrocarbon production for active margins. These include (1) a thick accretionary prism, (2) a thick incoming sedimentary section, (3) substantial axial trench sedimentation fed with continental detritus, (4) the development of decollement near the top of the incoming section, and (5) slow to moderate convergence rates. Based on geologic features observed in the seismic reflection profiles in the study area, the northern segment of the Manila Trench satisfies the conditions mentioned. A well-developed frontal wedge is evident from 18°N to 20°N formed from the accretion of the thick, continent-derived sedimentary cover of the incoming South China Sea slab (Fig. 1). Aside from this, the sediments accreted in the frontal wedge are also sourced from trench infill, which is fed by sediments derived from the continent-arc collision zones in SW Taiwan and Central Philippines (Hayes and Lewis, 1985). The numerous thrust faults in the accretionary prism also seem to converge into a decollement at the base of the wedge, which may have served as a well-developed fluid migration system. At the same time, Hayes and Lewis (1985) estimate a relatively slow convergence rate of 1 cm/yr for the trench. However, more recent estimates suggest a faster convergence rate. Estimates ranging from >70 mm/yr at ~19°N to 20 mm/yr to the south were reported by Hamburger et al. (2010). A faster convergence rate of 90–100 mm/yr was estimated by Qiu et al. (2019).

Initial results of the study indicate the possibility of widespread gas hydrates in the northern segment of the Manila Trench frontal wedge. The steady sediment supply from the Eurasian margin and the active collision in the Taiwan region are preconditions for methane gas generation. These organic-rich sediments overlying the subducting South

China Sea oceanic crust are accreted into the frontal wedge. Upward fluid expulsion due to convergence creates favorable conditions for gas hydrate formation. The imbricate frontal thrust faults appear to function as fluid conduits through which free gas migrates into shallow levels and crystallizes into clathrates (Fig. 10a). Based on the seismic sections, the NLT shows the limited distribution of BSRs. This may imply low sedimentation and organic matter supply, limiting viable methane sources within the basin. The basin fill of the NLT is mainly sourced from the Luzon arc, with some mass transport deposits sourced from the collapse of the frontal wedge. Surface samples from the basin were reported to be enriched in smectite, mainly transported as suspended sediment loads by surface currents (Liu et al., 2010). These were transported through the onshore fluvial systems draining into the forearc basin and are products of alteration of the andesitic-basaltic volcanic rocks in the Luzon arc (Liu et al., 2010). Sediments derived from the SW Taiwan collision zone are mainly deposited to the west of the frontal wedge via gravity-driven processes along the Gaoping submarine canyon. However, a recent study by Wang et al. (2022) suggests some terrigenous contribution from SE Taiwan, transported by deep-sea currents towards the south along Luzon Strait. However, for the NLT, arc-derived sediments are inferred to be more dominant due to the sediment transport by fluvial and submarine canyon systems situated east of the basin. Recent tectonic models also propose a proto-South China Sea (pro-SCS) affinity for the western Philippine seaboard (Yumul et al., 2020). This origin of the inferred basement may also explain the lack of deeper hydrocarbon sources in the NLT, with fluid migration along the landward-tilted sedimentary sequences resulting in the limited concentration of the inferred gas hydrates at the western portions of the

basin (Fig. 10a).

To the south, gas hydrates are inferred to be present mainly in the WLT infill (Fig. 10b). Double BSRs may also indicate the presence of heavy hydrocarbon gas fractions. However, its proximity to the Stewart Bank might also suggest disequilibrium conditions resulting from the effects of heat advection along structures and the rapid uplift experienced by the area. Sediments in the eastern South China Sea basin south of the Scarborough Seamount Chain are mainly sourced from the active Luzon arc with minor contributions from the Eurasian margin. The marked absence of BSRs west of the WLT may indicate the role of gas hydrate dissociation in the instability of the frontal prism slope. The eroded inner trench slope is probably associated with seepage-related slope failure, similar to what is observed in the Southern Cascadia wedge and northern Hispaniola margin (Orange and Breen, 1992). The compaction of accreting sediments leads to overpressure conditions, promoting fluid flow, which, combined with the oversteepening of slopes due to frontal wedge folding and thrusting, results in slope failure (Orange and Breen, 1992). Similar to what is inferred for the Shenhu area in the work of Wan et al. (2022), we infer that these mass wasting events lead to the gradual dissociation of gas hydrates, which may eventually contribute to succeeding slope failures (e.g., Huang et al., 2022; Wan et al., 2022). At the same time, the incoming South China Sea crust in this area has a thinner sedimentary cover and numerous bathymetric highs, further promoting the erosion of the frontal wedge. The preferential formation of gas hydrates within the WLT points to gas sources within the forearc basin. It is worth noting that previous tectonic models suggest a continental or continent-derived basement for the WLT, with sediments of continental provenance in the deeper parts of the

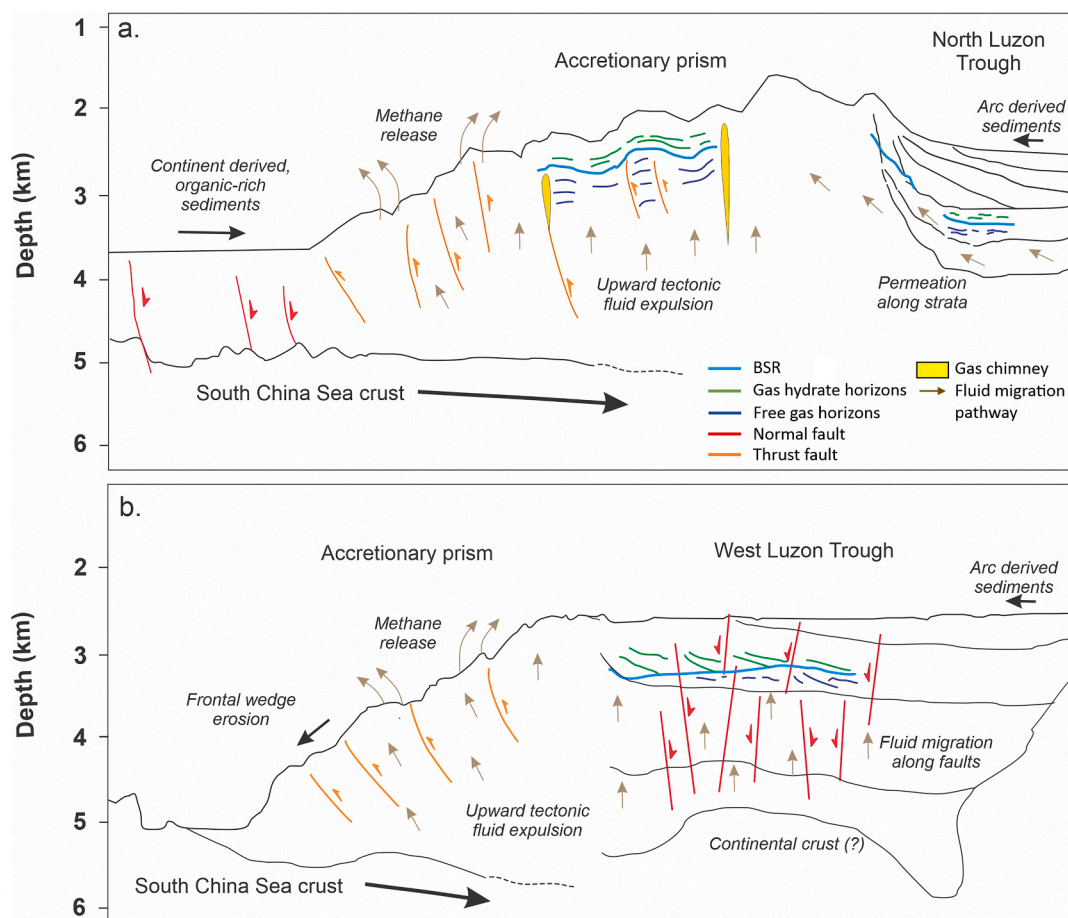


Fig. 10. Gas hydrate formation mechanisms in the identified possible accumulation sites in the Manila Trench region. (a) In the northern segment, accumulation is mainly within the accretionary prism, driven by fluid transport along thrust faults and gas chimneys. (b) To the south, gas hydrate indicators concentrate within the West Luzon Trough infill, with normal faults serving as dominant migration pathways.

the forearc basin (Arfai et al., 2011). This links the system to the Palawan Micro-continental Block, colliding with the Philippine Mobile Belt. Early middle Miocene or pre-Miocene source rocks are inferred for this basin based on onshore correlations.

6. Conclusions

The possible accumulation of gas hydrates in the Manila Trench forearc region is indicated by the occurrence of bottom simulating reflectors, enhanced amplitude reflectors, and gas chimneys associated with significant fluid migration along faults in the forearc. The prevalence of continuous BSRs indicates a possible fine-grained reservoir for the gas hydrates in the Manila Trench forearc region offshore western Luzon. Double BSRs, especially near the Stewart Bank, suggest two possible scenarios: the presence of a layered gas hydrate structure, indicating the influence of thermogenic gas sources, or an ongoing re-equilibration linked with rapid forearc uplift due to ridge subduction along the Scarborough Seamount Chain. Plumbing BSRs suggest significant thermogenic gas sources at depth and preferential accumulation in zones characterized by vertical fluid migration structures related to the ongoing subduction.

Forearc processes significantly influence the distribution of gas hydrate indicators in the Manila Trench forearc. At the northern segment, dominant subduction processes include accretion along the frontal wedge and arc-derived sedimentation in the North Luzon Trough. The accretion of continent-derived sediments provides hydrocarbon sources. It promotes the formation of thrust faults, leading to a more pronounced fluid transport that forms the widespread continuous BSRs and EARs within the accretionary prism. Fluid migration along the landward tilted sedimentary sequences of the North Luzon Trough further contributes hydrocarbon-rich fluids needed for gas hydrate formation in the accretionary prism and western portions of the basin. South of the Stewart Bank, gas hydrate accumulation is evidenced by continuous BSRs and EARs within the West Luzon Trough. Fluid migration is facilitated by the normal faults cutting through the basin fill, with continent-derived source rocks inferred for the basin.

Author contributions

Conceptualization: Leo Armada, Shu-Kun Hsu, Carla Dimalanta; Formal analysis: Elisha Jane Maglalang, Madeleine Santos, Karla May Sayen; Writing - original draft preparation: Elisha Jane Maglalang, Madeleine Santos, Karla May Sayen, Leo Armada; Writing - review and editing: Elisha Jane Maglalang, Karla May Sayen, Leo Armada, Carla Dimalanta, Graciano Yumul Jr., Shu-Kun Hsu.

Declaration of competing interest

The authors declare that they have no known competing financial interests or personal relationships that could have appeared to influence the work reported in this paper.

Data availability

The authors do not have permission to share data.

Acknowledgment

The authors would like to acknowledge the financial support the Taiwan Ministry of Science and Technology provided for the "Second Phase of the Philippines-Taiwan Integrated Geodynamics Project." Support provided by the Office of the Vice President for Academic Affairs of the University of the Philippines under the Energy Research Fund Program is also acknowledged. Fruitful discussions with members of the Rushurgent Working Group are also gratefully acknowledged.

References

- Arfai, J., Franke, D., Gaedicke, C., Lutz, R., Schnabel, M., Ladage, S., Berglar, K., Aurelio, M., Montano, J., Pellejera, N., 2011. Geological evolution of the West Luzon basin (south China sea, Philippines). *Mar. Geophys. Res.* 32, 349–362.
- Armada, L.T., Hsu, S.-K., Dimalanta, C.B., Yumul Jr., G.P., Doo, W.-B., Yeh, Y.-C., 2020. Forearc structures and deformation along the Manila Trench. *J. Asian Earth Sci.* 4, 100036 <https://doi.org/10.1016/j.jaesx.2020.100036>.
- Bautista, B.C., Bautista, M.L.P., Oike, K., Wu, F.T., Punongbayan, R.S., 2001. A new insight on the geometry of subducting slabs in northern Luzon, Philippines. *Tectonophysics* 339 (3–4), 279–310. [https://doi.org/10.1016/S0040-1951\(01\)00120-2](https://doi.org/10.1016/S0040-1951(01)00120-2).
- Bellon, H., Yumul Jr., G.P., 2000. Mio-Pliocene magmatism in the Baguio Mining District (Luzon, Philippines): age clues to its geodynamic setting. *Earth Planet Sci* 331, 295–302. [https://doi.org/10.1016/S1251-8050\(00\)01415-4](https://doi.org/10.1016/S1251-8050(00)01415-4).
- Berndt, C., Chi, W.-C., Jegen, M., Lebas, E., Crutchley, G., Muf, S., Hölz, S., Sommer, M., Lin, S., Liu, C.-S., Lin, A.T., Klaeschen, D., Klauke, I., Chen, L., Hsu, H.-H., Kunath, P., Elger, J., McIntosh, K.D., Feseker, T., 2019. Tectonic controls on gas hydrate distribution off SW Taiwan. *J. Geophys. Res. Solid Earth* 124 (2), 1164–1184. <https://doi.org/10.1029/2018JB016213>.
- Bohrmann, G., Torres, M.E., 2016. Marine gas hydrates. In: Harff, J., Meschede, M., Petersen, S., Thiede, J. (Eds.), *Encyclopedia of Marine Geosciences*. Encyclopedia of Earth Sciences Series. Springer Netherlands, pp. 433–437. https://doi.org/10.1007/978-94-007-6644-0_168-2.
- Boswell, R., Shipp, C., Reicher, T., Shelander, D., Saeki, T., Frye, M., Shedd, W., Collet, T. S., McConnell, D.R., 2016. Prospecting for marine gas hydrate resources. *Interpretation* 4 (1), SA13–SA24. <https://doi.org/10.1190/int-2015-0036.1>.
- Breen, N.A., Orange, D.L., 1992. The effects of fluid escape on accretionary wedges 1. Variable porosity and wedge convexity. *J. Geophys. Res. Solid Earth* 97 (B6), 9265–9275.
- Chen, M.A.P., Riedel, M., Hyndman, R.D., Dosso, S.E., 2007. AVO inversion of BSRs in marine gas hydrate studies. *Geophysics* 72 (2), C31–C43.
- Chen, S., Hsu, S., Wang, Y., Chung, S., Chen, P., Tsai, C., Liu, C., Lin, H., Lee, Y., 2014. Distribution and characters of the mud diapirs and mud volcanoes off southwest Taiwan. *J. Asian Earth Sci.* 92 <https://doi.org/10.1016/j.jseas.2013.10.009>.
- Chen, P.F., Olaverie, E.A., Wang, C.W., Bautista, B.C., Solidum Jr., R.U., Liang, W.T., 2015. Seismotectonics of Mindoro, Philippines. *Tectonophysics* 640, 70–79. <https://doi.org/10.1016/j.tecto.2014.11.023>.
- Chi, W.-C., Reed, D.L., Liu, C.-S., Lundberg, N., 1998. Distribution of the bottom-simulating reflector in the offshore Taiwan collision zone. *Terr. Atmos. Ocean Sci.* 9, 779–794.
- Demirbas, A., 2010. Methane Gas Hydrate: as a natural gas source. In: *Methane Gas Hydrate*. Green Energy and Technology. Springer, London, pp. 113–160. https://doi.org/10.1007/978-1-84882-872-8_4.
- Dhakal, S., Gupta, I., 2020. Predictive modeling of thermogenic methane hydrate formation and geobody distribution - results from numerical simulations. *J. Nat. Gas Sci. Eng.* 74, 103154 <https://doi.org/10.1016/j.jngse.2020.103154>.
- Dirgantara, F., Lin, A.T.-S., Liu, C.-S., Lin, C.-C., Chen, S.-C., 2020. Gas-hydrate systems and gas volumetric assessment in the Lower Fangliao Basin, Taiwan accretionary wedge. *J. Petrol. Geol.* 43 (1), 27–47. <https://doi.org/10.1111/jpg.12748>.
- Eng, C., Tsuji, T., 2019. Influence of faults and slumping on hydrocarbon migration inferred from 3D seismic attributes: Sanriku-Oki forearc basin, northeast Japan. *Mar. Petrol. Geol.* 99, 175–189. <https://doi.org/10.1016/j.marpetgeo.2018.10.013>.
- Fan, J., Zhao, D., Dong, D., 2016. Subduction of a buoyant plateau at the Manila Trench: tomographic evidence and geodynamic implications. *G-cubed* 17 (2), 571–586. <https://doi.org/10.1002/2015GC006201>.
- Floodgate, G.D., Judd, A.G., 1992. The origins of shallow gas. *Continental Shelf Res.* 12 (10), 1145–1156.
- Foucher, J.-P., Nouze, H., Henry, P., 2002. Observation and tentative interpretation of a double BSR on the Nankai slope. *Mar. Geol.* 187 (1–2), 161–175. [https://doi.org/10.1016/S0025-3227\(02\)00264-5](https://doi.org/10.1016/S0025-3227(02)00264-5).
- Geissler, W.H., Pulm, P.V., Jokat, W., Gebhart, A.C., 2014. Indications for the occurrence of gas hydrates in the Fram Strait from heat flow and multichannel seismic reflection data. *J. Geol. Res.* 3, 1–12. <https://doi.org/10.1155/2014/582424>.
- Golmshokt, A.Y., Soloviev, V.A., 2006. Some remarks on the thermal nature of the double BSR. *Mar. Geol.* 229 (3–4), 187–198. <https://doi.org/10.1016/j.margeo.2006.03.004>.
- Hamburger, M.W., Galgana, G.A., Bacolcol, T., McCaffrey, R., Yu, S., 2010. Analysis of oblique plate convergence along the Manila Trench and the Philippine trench. AGU Fall Meeting Abstracts 2010, T51D–T2084.
- Han, W.-C., Chen, L., Liu, C.-S., Berndt, C., Chi, W.-C., 2019. Seismic analysis of the gas hydrate system at Pointer Ridge offshore SW Taiwan. *Mar. Petrol. Geol.* 105, 158–167. <https://doi.org/10.1016/j.marpetgeo.2019.04.028>.
- Hayes, D., 2015. Multi-Channel seismic shot data from the Philippine Sea acquired during the R/V vema expedition V3613. IEDA. <https://doi.org/10.1594/IEDA/317105>, 1980.
- Hayes, D.E., Lewis, S.D., 1985. Structure and tectonics of the Manila Trench system, western Luzon, Philippines. *Energy* 10 (3–4), 263–279. [https://doi.org/10.1016/0360-5442\(85\)90046-5](https://doi.org/10.1016/0360-5442(85)90046-5).
- He, J., Wang, S., Zhang, W., Yan, W., Lu, Z., 2016. Characteristics of mud diapirs and mud volcanoes and their relationship to oil and gas migration and accumulation in a marginal basin of the northern South China Sea. *Environ. Earth Sci.* 75 (15) <https://doi.org/10.1007/s12665-016-5894-9>.
- Hsu, Y.-J., Yu, S.-B., Song, T.-R.A., Bacolcol, T., 2012. Plate coupling along the Manila subduction zone between Taiwan and northern Luzon. *J. Asian Earth Sci.* 51 (2), 98–108. <https://doi.org/10.1016/j.jseas.2012.01.005>.

- Hsu, H.-H., Liu, C.-S., Morita, S., Tu, S.-L., Lin, S., Machiyama, H., Azuma, W., Ku, C.-Y., Chen, S.-C., 2018. Seismic imaging of the Formosa Ridge cold seep site offshore of southwestern Taiwan. *Mar. Geophys. Res.* 39, 523–535. <https://doi.org/10.1007/s11001-017-9339-y>.
- Huang, Y., Cheng, J., Wang, M., Wang, S., Yan, W., 2022. Gas hydrate dissociation events during LGM and their potential trigger of submarine landslides: foraminifera and geochemical records from two Cores in the Northern South China Sea. *Front. Earth Sci.* 10, 876913 <https://doi.org/10.3389/feart.2022.876913>.
- Huang, C.Y., Wang, P., Yu, M., You, C.F., Liu, C.S., Zhao, X., et al., 2019. Potential role of strike-slip faults in opening up the South China Sea. *Natl. Sci. Rev.* 6 (5), 891–901.
- Huang, Y.S., Hsu, S.K., Su, C.C., Lin, A.T.S., Yu, P.S., Babonneau, N., et al., 2021. Shallow gas hydrates off southwest Taiwan and their mechanisms. *Mar. Geophys. Res.* 42 (1), 1–12.
- Hyndman, R.D., Davis, E.E., 1992. A mechanism for the formation of methane hydrate and seafloor bottom-simulating reflectors by vertical fluid expulsion. *J. Geophys. Res.* 97 (B5), 7025–7041. <https://doi.org/10.1029/91JB03061>.
- Hyndman, R.D., Wang, K., Yuan, T., Spence, G.D., 1993. Tectonic sediment thickening: fluid expulsion and the thermal regime of subduction zone accretionary prisms: the Cascadia Margin off Vancouver Island. *J. Geophys. Res.* 98, 21865–21876.
- Judd, A., Hovland, M., 2007. *Seabed Fluid Flow: The Impact on Geology, Biology, and the Marine Environment*. Cambridge University Press.
- Karig, D.E., 1983. Accreted terranes in the northern part of the Philippine Archipelago. *Tectonics* 2 (2), 211–236. <https://doi.org/10.1029/TC002i002p00211>.
- Katz, B.J., 2011. Microbial processes and natural gas accumulations. *Open Geol. J.* 5 (1).
- Katz, B.J., Narimanov, A., Huseinzadeh, R., 2002. Significance of microbial processes in gases of the South Caspian basin. *Mar. Petrol. Geol.* 19 (6), 783–796. [https://doi.org/10.1016/S0264-8172\(02\)00086-7](https://doi.org/10.1016/S0264-8172(02)00086-7).
- Kret, K., Tsuji, T., Chhun, C., Takano, O., 2020. Distributions of gas hydrate and free gas accumulations associated with fluid flow in the Sanriku-Oki forearc basin, northeast Japan. *Mar. Petrol. Geol.* 116, 104305 <https://doi.org/10.1016/j.marpetgeo.2020.104305>.
- Kvenvolden, K.A., 1993. Gas hydrates – Geological perspective and global change. *Rev. Geophys.* 31 (2), 173–187. <https://doi.org/10.1029/93RG00268>.
- Kvenvolden, K.A., 1988. Methane hydrate—a major reservoir of carbon in the shallow geosphere? *Chem. Geol.* 71 (1–3), 41–51. [https://doi.org/10.1016/0009-2541\(88\)90104-0](https://doi.org/10.1016/0009-2541(88)90104-0).
- Kvenvolden, K.A., Claypool, G.E., Threlkeld, C.N., Sloan, E.D., 1984. Geochemistry of a naturally occurring massive marine gas hydrate. *Org. Geochem.* 6, 703–713. [https://doi.org/10.1016/0146-6380\(84\)90091-3](https://doi.org/10.1016/0146-6380(84)90091-3).
- Kvenvolden, K.A., McMenamin, M.A., 1980. Hydrates of natural gas: a review of their geologic occurrence. In: *United States Geological Survey Circular*, vol. 825. United States Department of the Interior Publication, USA., p. 11
- Lewis, S.D., Hayes, D.E., 1984. A geophysical study of the Manila Trench, Luzon, Philippines: 2. Fore arc basin structural and stratigraphic evolution. *J. Geophys. Res.* 89 (B11), 9196–9214. <https://doi.org/10.1029/jb089ib11p09196>.
- Liang, J., Zhang, W., Lu, J.A., Wei, J., Kuang, Z., He, Y., 2019. Geological occurrence and accumulation mechanism of natural gas hydrates in the eastern Qiongdongnan Basin of the South China Sea: insights from site MGSS-W9-2018. *Mar. Geol.* 418, 106042.
- Liao, W.Z., Lin, A.T., Liu, C.S., Oung, J.N., Wang, Y., 2014. Heat flow in the rifted continental margin of the South China Sea near Taiwan and its tectonic implications. *J. Asian Earth Sci.* 92, 233–244. <https://doi.org/10.1016/j.jseas.2014.01.003>.
- Li, L., Liu, H., Zhang, X., Lei, X., Sha, Z., 2015. BSRs, estimated heat flow, hydrate-related gas volume and their implications for methane seepage and gas hydrate in the Dongsha region, northern South China Sea. *Mar. Petrol. Geol.* 67, 785–794. <https://doi.org/10.1016/j.marpetgeo.2015.07.008>.
- Ligtenberg, J.H., 2005. Detection of fluid migration pathways in seismic data: implications for fault seal analysis. *Basin Res.* 17 (1), 141–153. <https://doi.org/10.1111/j.1365-2117.2005.00258.x>.
- Liu, Z., Colin, C., Li, X., Zhao, Y., Tuo, S., Chen, Z., et al., 2010. Clay mineral distribution in surface sediments of the northeastern South China Sea and surrounding fluvial drainage basins: source and transport. *Mar. Geol.* 277 (1–4), 48–60.
- Lu, Y., Luan, X., Lyu, F., Wang, B., Yang, Z., Yang, T., Yao, G., 2017. Seismic evidence and formation mechanism of gas hydrates in the Zhongjiannan Basin, Western margin of the South China Sea. *Mar. Petrol. Geol.* 84, 274–288. <https://doi.org/10.1016/j.marpetgeo.2017.04.005>.
- Matsumoto, R., Ryu, B.-J., Lee, S.-R., Lin, S., Wu, S., Sain, K., Pecher, I., Riedel, M., 2011. Occurrence and exploration of gas hydrate in the marginal seas and continental margin of the Asia and Oceania region. *Mar. Petrol. Geol.* 28 (10), 1751–1767. <https://doi.org/10.1016/j.marpetgeo.2011.09.009>.
- Meslé, M., Dromart, G., Oger, P., 2013. Microbial methanogenesis in subsurface oil and coal. *Res. Microbiol.* 164 (9), 959–972.
- Mishra, C.K., Dewangan, P., Sriram, G., Kumar, A., Dakara, G., 2020. Spatial Distribution of gas hydrate deposits in Krishna-Godavari offshore basin, Bay of Bengal. *Mar. Petrol. Geol.* 112, 104037 <https://doi.org/10.1016/j.marpetgeo.2019.104037>.
- Miyakawa, A., Saito, S., Yamada, Y., Tomaru, H., Kinoshita, M., Tsuji, T., 2014. Gas hydrate saturation at site C 0002, IODP expeditions 314 and 315, in the Kumano Basin, Nankai Trough. *Isl. Arc* 23 (2), 142–156. <https://doi.org/10.1111/iar.12064>.
- Nasif, A., Ozel, F.E., Dondurur, D., 2020. Seismic identification of gas hydrates: a case study from Sakarya Canyon, western Black Sea. *Turk. J. Earth Sci.* 29 (3), 434–454. <https://doi.org/10.3906/yer-1909-2>.
- Nixon, M.F., Grozic, J.L., 2007. Submarine slope failure due to gas hydrate dissociation: a preliminary quantification. *Can. Geotech. J.* 44 (3), 314–325. <https://doi.org/10.1139/t06-121>.
- Orange, D.L., Breen, N.A., 1992. The effects of fluid escape on accretionary wedges 2. Seepage force, slope failure, headless submarine canyons, and vents. *J. Geophys. Res. Solid Earth* 97 (B6), 9277–9295.
- Paganoni, M., Cartwright, J.A., Foschi, M., Shipp, C.R., Rensbergen, P.V., 2018. Relationship between fluid-escape pipes and hydrate distribution in offshore Sabah (NW Borneo). *Mar. Geol.* 395, 82–103. <https://doi.org/10.1016/j.margeo.2017.09.010>.
- Portnov, A., Cook, A.E., Sawyer, D.E., Yang, C., Hillman, J.I.T., Waite, W.F., 2019. Clustered BSRs: evidence for gas hydrate-bearing turbidite complexes in folded regions, example from the Perdido Fold Belt, northern Gulf of Mexico. *Earth Planet Sci. Lett.* 528, 115843 <https://doi.org/10.1016/j.epsl.2019.115843>.
- Posewang, J., Mienert, J., 1999. The enigma of double BSRs: indicators for change in the hydrate stability field. *Geo Mar. Lett.* 19, 157–163. <https://doi.org/10.1007/s003670050103>.
- Qiu, Q., Li, L., Hsu, Y.J., Wang, Y., Chan, C.H., Switzer, A.D., 2019. Revised earthquake sources along Manila trench for tsunami hazard assessment in the South China Sea. *Nat. Hazards Earth Syst. Sci.* 19 (7), 1565–1583.
- Rajput, S., Thakur, N.K., 2016. *Fluid flows. In: Geologic Controls for Gas Hydrate Formations and Unconventionals*. Elsevier, Radarweg, Amsterdam, pp. 165–193.
- Reed, D.W., Fujita, Y., Delwiche, M.E., Blackwelder, D.B., Sheridan, P.P., Uchida, T., Colwell, F.S., 2002. Microbial communities from methane hydrate-bearing deep marine sediments in a forearc basin. *Appl. Environ. Microbiol.* 68 (8), 3759–3770. <https://doi.org/10.1128/AEM.68.8.3759-3770.2002>.
- Riedel, M., Willoughby, E.C., Chopra, S. (Eds.), 2010. *Geophysical Characterization of Gas Hydrates*. Society of Exploration Geophysicists.
- Rogers, K.M., Collen, J.D., Johnston, J.H., Elgar, N.E., 1999. A geochemical appraisal of oil seeps from the East Coast Basin, New Zealand. *Org. Geochem.* 30 (7), 593–605. [https://doi.org/10.1016/S0146-6380\(99\)00036-4](https://doi.org/10.1016/S0146-6380(99)00036-4).
- Sain, K., Gupta, H., 2012. Gas hydrates in India: potential and development. *Gondwana Res.* 22 (2), 645–657. <https://doi.org/10.1016/j.gr.2012.01.007>.
- Sandwell, D.T., Smith, W.H.F., Becker, J.J., 2014. SRTM30+ Global 1-km Digital Elevation Model (DEM): Version 11: Land Surface. Distributed by the Pacific Islands Ocean Observing System (PacIOOS). http://pacioos.org/metadata/srtm30plus_v11_land.html. (Accessed 8 January 2021).
- Shedd, W., Boswell, R., Frye, M., Godfriaux, P., Kramer, K., 2012. Occurrence and nature of “bottom simulating reflectors” in the northern Gulf of Mexico. *Mar. Petrol. Geol.* 34 (1), 31–40. <https://doi.org/10.1016/j.marpetgeo.2011.08.005>.
- Shi, X., Qiu, X., Xia, K., Zhou, D., 2003. Characteristics of surface heat flow in the South China Sea. *J. Asian Earth Sci.* 22 (3), 265–277.
- Shibley, T.H., Houston, M.H., Buffler, R.T., Shaub, F.J., Mcmillen, K.J., Laod, J.W., Worzel, J.L., 1979. Seismic evidence for widespread possible gas hydrate horizons on continental slopes and rises. *Am. Assoc. Petrol. Geol. Bull.* 63 (12), 2204–2213.
- Shyu, C.T., Yu-Jhong, C., Chiang, S.T., Liu, C.S., 2006. Heat flow measurements over bottom simulating reflectors, offshore southwestern Taiwan. *Terr. Atmos. Ocean Sci.* 17 (4), 845.
- Sloan, Jr., E.D., 1998. *Clathrate of Hydrates of Natural Gases*, second ed. Marcel Dekker, Inc., New York.
- Stevenson, A.J., 1996. Generation, migration and resource potential for hydrocarbons in accretionary subduction systems: a large unconventional hydrocarbon resource? In: *Howell, D.G. (Ed.), The Future of Energy Gases*, USGS, Numbered Series 1590. Professional paper, Washington United States Government Printing Office, pp. 353–363.
- Suzuki, K., Schultheiss, P., Nakatsuka, Y., Ito, T., Egawa, K., Holland, M., Yamamoto, K., 2015. Physical properties and sedimentological features of hydrate-bearing samples recovered from the first gas hydrate production test site on Daini-Atsumi Knoll around eastern Nankai Trough. *Mar. Petrol. Geol.* 66, 346–357. <https://doi.org/10.1016/j.marpetgeo.2015.02.025>.
- Taladay, K., Boston, B., Moore, G., 2017. Gas-in-place estimate for potential gas hydrate concentrated zone in the Kumano Basin, Nankai Trough Forearc, Japan. *Energies* 10 (10), 1552. <https://doi.org/10.3390/en10101552>.
- Tinivella, U., Giustiniani, M., 2013. Variations in BSR depth due to gas hydrate stability versus pore pressure. *Global Planet. Change* 100, 119–128. <https://doi.org/10.1016/j.gloplacha.2012.10.012>.
- Tissot, B.P., Welte, D.H., 1984. *Petroleum Formation and Occurrence*. Springer-Verlag, Berlin. <https://doi.org/10.1007/978-3-642-87813-8>.
- Wan, Z.F., Zhang, W., Ma, C., Liang, J.Q., Li, A., Meng, D., Sun, Y.F., 2022. Dissociation of gas hydrates by hydrocarbon migration and accumulation-derived slope failures: an example from the South China Sea. *Geosci. Front.* 13 (2), 101345 <https://doi.org/10.1016/j.gsf.2021.101345>.
- Wang, C., Cui, H., Zeng, L., Su, M., 2022. Provenance of sediments in the northern Manila Trench: an assessment from detrital zircon geochronology. *Sci. China Earth Sci.* 1–13.
- Wang, S., Yan, W., Song, H., 2006. Mapping the thickness of the gas hydrate stability zone in the South China Sea. *Terr. Atmos. Ocean Sci.* 17 (4), 815. <https://doi.org/10.3319/tao.2006.17.4.815> (gh).
- Wu, S., Zhang, G., Huang, Y., Liang, J., Wong, H.K., 2005. Gas hydrate occurrence on the continental slope of the northern South China Sea. *Mar. Petrol. Geol.* 22 (3), 403–412. <https://doi.org/10.1016/j.marpetgeo.2004.11.006>.
- Yang, T.F., Lee, T., Chen, C.-H., Cheng, S.-N., Knittel, U., Punongbayan, R.S., Rasdas, A. R., 1996. A double island arc between Taiwan and Luzon: consequence of ridge subduction. *Tectonophysics* 258 (1–4), 85–101. [https://doi.org/10.1016/0040-1951\(95\)00180-8](https://doi.org/10.1016/0040-1951(95)00180-8).
- Yuan, T., Spence, G.D., Hyndman, R.D., Minshull, T.A., Singh, S.C., 1999. Seismic velocity studies of a gas hydrate bottom-simulating reflector on the northern Cascadia continental margin: amplitude modeling and full waveform inversion. *J. Geophys. Res. Solid Earth* 104 (B1), 1179–1191.
- Yumul Jr., G.P., Dimalanta, C.B., Tamayo, R.A., Maury, R.C., 2003. Collision, subduction and accretion events in the Philippines: a synthesis. *Isl. Arc* 12 (2), 77–91. <https://doi.org/10.1046/j.1440-1738.2003.00382.x>.

- Yumul Jr., G.P., Dimalanta, C.B., Maglambayan, V.B., Marquez, E.J., 2008. Tectonic setting of a composite terrane: a review of the Philippine island arc system. *Geosci. J.* 12 (1), 7–17.
- Yumul Jr., G.P., Dimalanta, C.B., Gabo-Ratio, J.A.S., Queaño, K.L., Armada, L.T., Padrones, J.T., et al., 2020. Mesozoic rock suites along western Philippines: exposed proto-South China Sea fragments? *J. Asian Earth Sci.* X 4, 100031.
- Zhang, W., Liang, J., Wei, J., Lu, J., Su, P., Lin, L., Huang, W., Guo, Y., Deng, W., Yang, X., Wan, Z., 2020. Geological and geophysical features of and controls on occurrence and accumulation of gas hydrates in the first offshore gas-hydrate production test region in the Shenhu area, Northern South China Sea. *Mar. Petrol. Geol.* 114, 104191 <https://doi.org/10.1016/j.marpetgeo.2019.104191>.
- Zhang, F., Lin, J., Zhou, Z., Yang, H., Zhan, W., 2018. Intra- and intertrench variations in flexural bending of the Manila, Mariana and global trenches: implications on plate weakening in controlling trench dynamics. *Geophys. J. Int.* 212 (2), 1429–1449. <https://doi.org/10.1093/gji/ggx488>.